PAPER

Extended One-Shot Decorrelating Detector for Asynchronous DS/CDMA Systems

Jee Woong KANG[†a)], ***Student Member and*** **Kwang Bok (Ed) LEE**[†], ***Nonmember***

SUMMARY We propose an extended one-shot decorrelating detector (EOS-DD) which may be viewed as a generalized double window multiuser detector (DW-MD) for asynchronous direct-sequence code-division multiple-access (DS/CDMA) systems in frequency selective fading environments. The EOS-DD extends a processing window and the received signal over an extended window is utilized for decorrelating. The effects of the window size on BER performance are investigated by numerical analysis. Analysis and simulation show that the EOS-DD is superior to the one-shot decorrelating detector (OS-DD) and finite memory length truncated decorrelating detector (FIR-DD) in terms of noise enhancement and near-far resistance. It is also shown that the EOS-DD with window size 4 can provide significantly improved performance compared to the EOS-DD with window size 2.

key words: *multiuser detector, decorrelator, CDMA, asynchronous system*

1. Introduction

Next generation communication systems such as International Mobile Telecommunications - 2000 (IMT-2000) have been developed to support voice, data, and multimedia services with large system capacity. A direct-sequence code-division multiple-access (DS/CDMA) scheme has been chosen as a multiple access technique for next generation communication systems. A conventional matched filter (MF) detector for DS/CDMA systems is designed for single user environments. To overcome such a limitation, multiuser detectors have been investigated for next generation communication systems.

Since Verdú investigated the optimal multiuser detector for multiuser environment [1], [2], various types of multiuser detectors have been proposed [3]–[7]. In the class of linear multiuser detectors, the decorrelating detector [3], [4] has received a lot of attention because it is robust to near-far effect and does not need channel information. In decorrelating detector, the received signal is matched-filtered by spreading sequence corresponding to each user, and processed by decorrelator to eliminate multiple access interference (MAI). For synchronous systems, the decorrelating detector may eliminate MAI by processing a received signal over the present symbol duration. However, for asynchronous systems, the decorrelating detector needs an infinitely long processing window to eliminate MAI. Of course, this infinite memory length decorrelating detector (IIR-DD) [8] is almost impossible to implement due to its computational complexity, memory requirements, and processing delay. Therefore, several suboptimum decorrelating detectors for asynchronous systems have been proposed: a finite memory length truncated decorrelating detector (FIR-DD) [8], a one-shot decorrelating detector (OS-DD) [2], [9], and a double window multiuser detector (DW-MD) [10]. However, these schemes have some limitations, for example, severe noise enhancement and incomplete MAI elimination.

We propose an extended one-shot decorrelating detector (EOS-DD) which may be viewed as a generalization of the DW-MD. We develop the EOS-DD mathematically and show that the proposed EOS-DD reduces noise enhancement further by extending the processing window. The BER performance of the EOS-DD is investigated analytically and verified by computer simulation. Furthermore, the effects of the processing window size on performance are also investigated.

The paper is organized as follows. The system and channel models are presented in Sect. 2. In Sect. 3, the previously proposed detectors are described and the EOS-DD is proposed. The complexity issue is also discussed in Sect. 3. The performance of the EOS-DD and the effects of the window size on performance are investigated in Sect. 4. Numerical results are presented in Sect. 5, and finally conclusions are given in Sect. 6.

2. System and Channel Models

A system consisting of K users is considered. The channel for each user is modelled as a frequency selective fading channel with L resolvable paths. The fading characteristic for each path is independent and identically distributed. It is assumed that the fading rate is slow enough to regard the channel characteristic as constant over one symbol duration T_s. Then, the received signal $r(t)$ can be represented as follows:

$$r(t)=\sum_{i=-\infty}^{\infty}\sum_{k=1}^{K}\sum_{l=1}^{L}h_{k,l}(i)d_k(i)s_k(t-iT_s-\tau_{k,l})+n(t) \quad (1)$$

Manuscript received January 30, 2002.
Manuscript revised September 24, 2002.

[†]The authors are with Seoul National University, Shinlim 9 Dong, Kwanak Gu, Seoul, Korea.
a) E-mail: kangjw@mobile.snu.ac.kr

where $h_{k,l}(i)$ is the k-th user's l-th path's channel impulse response at the i-th symbol duration, $d_k(i)$ represents the k-th user's data symbol at the i-th time, $s_k(t)$ is the k-th user's spreading sequence waveform which is zero outside $[0, T_s]$ and has unit energy, and $n(t)$ is zero-mean additive white Gaussian noise (AWGN) with variance σ^2. $\tau_{k,l}$ denotes the k-th user's l-th path's delay which is assumed to increase with l.

For notational convenience, (1) is expressed in vector form.

$$r(t) = \sum_{i=-\infty}^{\infty} \boldsymbol{s}(i;t)^T \cdot \boldsymbol{b}(i) + n(t), \tag{2}$$

where $\boldsymbol{s}(i,t)$ is a spreading sequence column vector which is defined as $[s_1(t - iT_s - \tau_{1,1}) \ \ldots \ s_1(t - iT_s - \tau_{1,L}) \ s_2(t - iT_s - \tau_{2,1}) \ \ldots \ s_K(t - iT_s - \tau_{K,L})]^T$ and $\boldsymbol{b}(i) \in \mathbb{C}^{KL\times 1}$ of which the $(kL+l)$-th element $b_{k,l}(i)$ is defined as $h_{k,l}(i)d_k(i)$. This is referred to as a channel-data vector.

3. Decorrelating Detector

3.1 The Previously Proposed Decorrelating Detectors

To explain basic concepts of the previously proposed decorrelating detectors, we consider a multiuser system with two user and single path propagation. To detect the i-th symbol for the first user, OS-DD uses received signal over a processing window corresponding to the desired symbol duration, as shown in Fig. 1 (a). Since parts of the second user's $(i-1)$-th and i-th symbols are superposed on the desired symbol, the received signal is processed by a full MF for the desired symbol and two partial MF for the interfering symbols, then three MF outputs are fed into decorrelator. Full MF and partial MF mean the matched filter processing the received signal during whole symbol duration, and during a part of symbol duration within the processing window, respectively. In general case of K users and L resolvable paths for each user's signal, OS-DD requires $(2KL-1)$ MFs. This OS-DD eliminates MAI completely. However, it provides poor performance owing to severe noise enhancement [9]. And, a separate decorrelator for each user and path is needed, which results in an increase in computational complexity.

To reduce the noise enhancement occurred in OS-DD, the decorrelating detector with the double window size has been proposed, and it is referred to DW-MD [10]. In Fig. 1(b), two full MFs for the ith symbols and four partial MFs for the $(i-1)$-th and $(i+1)$-th symbols are used to demodulate the i-th symbols. In general case, KL full MFs and $2KL$ partial MFs are required. By extending the processing window, perfor-

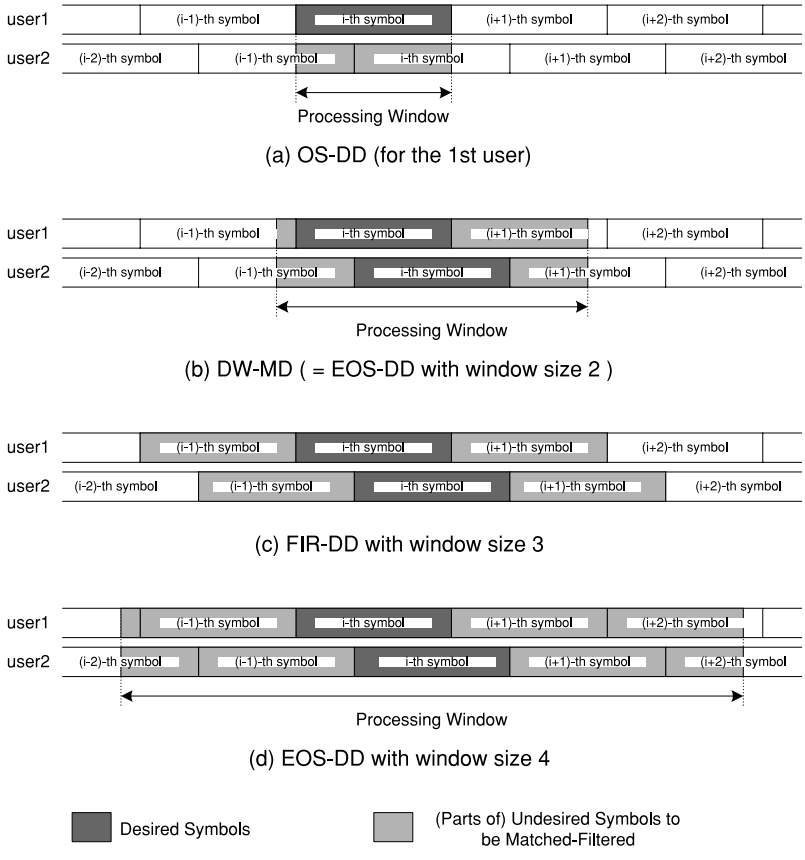

Fig. 1 Examples of OS-DD, DW-DD, FIR-DD and EOS-DD (K=2 and L=1).

mance degradation due to noise enhancement becomes smaller than that of OS-DD. And only one decorrelator is needed for all users and paths.

FIR-DD is an approximation of IIR-DD with finite memory length. As shown in Fig. 1(c), FIR-DD with window size $2W+1$ utilizes $(2W+1)KL$ full MFs where W is a positive integer (in Fig. 1(c), W is 1). However, there is residual MAI even after decorrelating process, which is known as the edge effect [8]. In this example, the $(i+2)$-th symbol of the first user and the $(i-2)$-th symbol of the second user act as residual MAI. Thus, the performance of FIR-DD may be degraded due to residual MAI.

3.2 Extended One-Shot Decorrelating Detector

In this subsection, we explain the configuration and process of the extended one-shot decorrelating detector. EOS-DD may be viewed as a generalization of DW-MD, and the basic operation of this detector is similar to that of DW-MD. However, the processing window size is generalized to $2W$ symbol duration, from $(i+1-W)T_s$ to $(i+1-W)T_s$, and consequently $2W+1$ MF outputs are generated for each user's each path. With the assumption of K users and L resolvable paths for each user signal, $(2W+1)KL$ MF outputs are utilized at decorrelating process.

Figure 2 shows the structure of EOS-DD. EOS-DD with window size $2W$ consists of $2W+1$ MF banks, a decorrelator, and K coherent combiners. Each MF bank is composed of KL MFs. At the $(W+1-q)$-th MF bank where q is an integer ranging from $-W+1$ to $W-1$, the received signal is matched-filtered by corresponding spreading sequence waveforms with one entire symbol duration. The MF output vector from the $(W+1-q)$-th MF bank, $\boldsymbol{r}(i-q)$, is defined as

$$\begin{aligned}\boldsymbol{r}(i-q) &\equiv \int_{-\infty}^{\infty} \boldsymbol{s}(i-q,t)r(t)dt \\ &= \mathbf{R}(1)\cdot\boldsymbol{b}(i-q-1)+\mathbf{R}(0)\cdot\boldsymbol{b}(i-q) \\ &\quad +\mathbf{R}(-1)\cdot\boldsymbol{b}(i-q+1)+\boldsymbol{n}(i-q), \quad (3)\end{aligned}$$

where $\mathbf{R}(1)$, $\mathbf{R}(0)$, and $\mathbf{R}(-1)$ are correlation matrices defined as

$$\begin{aligned}\mathbf{R}(1) &= \int_{-\infty}^{\infty} \boldsymbol{s}(i-1,t)\cdot\boldsymbol{s}(i,t)^T dt \\ \mathbf{R}(0) &= \int_{-\infty}^{\infty} \boldsymbol{s}(i,t)\cdot\boldsymbol{s}(i,t)^T dt \quad (4) \\ \mathbf{R}(-1) &= \int_{-\infty}^{\infty} \boldsymbol{s}(i,t)\cdot\boldsymbol{s}(i-1,t)^T dt,\end{aligned}$$

and $\boldsymbol{n}(i-q)\in\mathbb{C}^{KL\times 1}$ is the MF noise vector which is defined by $\int_{-\infty}^{\infty}\boldsymbol{s}(i-q,t)n(t)dt$ and its covariance matrix is

$$E[\boldsymbol{n}(i)\cdot\boldsymbol{n}(i)^H]=\sigma^2\mathbf{R}(0). \quad (5)$$

In the first MF bank, the received signal at the end of the processing window is processed by a set of parts of corresponding spreading sequence waveforms. These waveforms are called partial spreading sequence waveforms and they are expressed as

$$\begin{aligned}&\tilde{s}_k(t-(i-W)T_s-\tau_{k,l}) \\ &\equiv\begin{cases}s_k(t-(i-W)T_s-\tau_{k,l}), \\ \quad (i-W+1)T_s\le t<(i-W+1)T_s+\tau_{k,l} \\ 0, \quad \text{Otherwise.}\end{cases} \quad (6)\end{aligned}$$

The MF using partial spreading sequence waveforms is

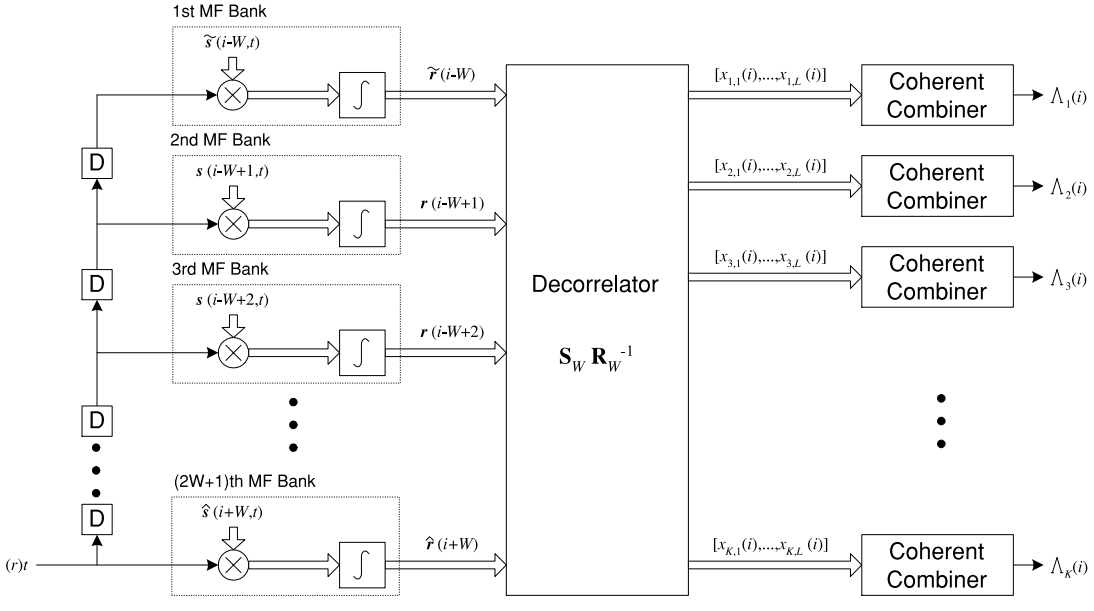

Fig. 2 Block diagram of the EOS-DD.

called a partial MF. This partial MF output vector is expressed as

$$\begin{aligned}\tilde{\boldsymbol{r}}(i\ -\ W) &\equiv \int_{-\infty}^{\infty} \tilde{\boldsymbol{s}}(i-W,t)r(t)dt \\ &= \tilde{\mathbf{R}}(0)\cdot\boldsymbol{b}(i-W) + \mathbf{R}(-1)\cdot\boldsymbol{b}(i-W+1) \\ &\quad +\tilde{\boldsymbol{n}}(i-W) \end{aligned} \tag{7}$$

where the tilde in $\tilde{\boldsymbol{s}}(i-W,t)$ means that its elements are partial spreading sequence waveforms instead of full spreading sequence waveforms. Note that there are two changes compared to (3). The first is that the partial correlation matrix $\tilde{\mathbf{R}}(0)$ which is defined as $\int_{-\infty}^{\infty}\tilde{\boldsymbol{s}}(i,t)\cdot\tilde{\boldsymbol{s}}(i,t)^T dt$ is used in (7) instead of the correlation matrix $\mathbf{R}(0)$. The second is that the $\mathbf{R}(1)\cdot\boldsymbol{b}(i-W-1)$ term is absent. Similarly, the last MF bank utilizes partial spreading sequence waveforms defined as

$$\begin{aligned}&\hat{s}_k(t-(i+W)T_s-\tau_{k,l}) \\ &\equiv \begin{cases} s_k(t-(i+W)T_s-\tau_{k,l}), \\ \quad (i+W)T_s+\tau_{k,l}\le t<(i+W+1)T_s \\ 0, \quad \text{Otherwise}, \end{cases}\end{aligned} \tag{8}$$

and its MF output vector is

$$\begin{aligned}\hat{\boldsymbol{r}}(i\ +\ W) &\equiv \int_{-\infty}^{\infty} \hat{\boldsymbol{s}}(i+W,t)r(t)dt \\ &= \mathbf{R}(1)\cdot\boldsymbol{b}(i+W-1) + \hat{\mathbf{R}}(0)\cdot\boldsymbol{b}(i+W) \\ &\quad +\hat{\boldsymbol{n}}(i+W), \end{aligned} \tag{9}$$

where $\hat{\mathbf{R}}(0)=\int_{-\infty}^{\infty}\hat{\boldsymbol{s}}(i,t)\cdot\hat{\boldsymbol{s}}(i,t)^T dt$. For notational convenience, all of the MF output vectors may be combined to form a vector $\mathbf{r}_W(i)\in\mathbb{C}^{(2W+1)KL\times 1}$, and may be expressed as

$$\begin{aligned}&\mathbf{r}_W(i) \\ &= [\tilde{\boldsymbol{r}}(i-W)^T\ \boldsymbol{r}(i-W+1)^T\ \ldots\ \hat{\boldsymbol{r}}(i+W)^T]^T \\ &= \int_{-\infty}^{\infty}\mathbf{s}_W(i,t)r(t)dt \\ &= \mathbf{R}_W\cdot\mathbf{b}_W(i)+\mathbf{n}_W(i), \end{aligned} \tag{10}$$

where

$$\begin{aligned}&\mathbf{s}_W(i,t) \\ &\equiv [\tilde{\boldsymbol{s}}(i-W,t)^T\ \boldsymbol{s}(i-W+1,t)^T\ldots\hat{\boldsymbol{s}}(i+W,t)^T]^T, \\ &\mathbf{b}_W(i) \\ &\equiv [\boldsymbol{b}(i-W)^T\ \boldsymbol{b}(i-W+1)^T\ldots\boldsymbol{b}(i+W)^T]^T, \\ &\mathbf{n}_W(i) \\ &\equiv [\tilde{\boldsymbol{n}}(i-W)^T\ \boldsymbol{n}(i-W+1)^T\ldots\hat{\boldsymbol{n}}(i+W)^T]^T, \\ &\mathbf{R}_W \equiv \int_{-\infty}^{\infty}\mathbf{s}_W(i,t)\cdot\mathbf{s}_W(i,t)^T dt \\ &= \begin{bmatrix} \tilde{\mathbf{R}}(0) & \mathbf{R}(-1) & \mathbf{0}_{KL\times KL} & \mathbf{0}_{KL\times KL} & \ldots \\ \mathbf{R}(1) & \mathbf{R}(0) & \mathbf{R}(-1) & \mathbf{0}_{KL\times KL} & \ldots \\ \mathbf{0}_{KL\times KL} & \mathbf{R}(1) & \mathbf{R}(0) & \mathbf{R}(-1) & \ldots \\ \ldots & \ldots & \ldots & \ldots & \ldots \\ \ldots & \mathbf{0}_{KL\times KL} & \mathbf{0}_{KL\times KL} & \mathbf{R}(1) & \hat{\mathbf{R}}(0) \end{bmatrix}, \end{aligned} \tag{11}$$

and $\mathbf{0}_{A\times B}$ is an $A\times B$ null matrix.

Since there are nonzero off-diagonal terms in $\mathbf{R}_W$, MAI exists in the MF output vector in (10). To eliminate MAI, the MF output vector is decorrelated by linear transformation $\mathbf{D}_W\in\mathbb{R}^{KL\times(2W+1)KL}$ which is defined as

$$\mathbf{D}_W \equiv \mathbf{S}_W\cdot\mathbf{R}_W^{-1}, \tag{12}$$

where $\mathbf{S}_W\equiv[\mathbf{0}_{KL\times WKL}\ \mathbf{I}_{KL\times KL}\ \mathbf{0}_{KL\times WKL}]$ selects the desired i-th symbols, and $\mathbf{I}_{A\times A}$ is a $A\times A$ identity matrix. Then, the decorrelator output vector $\boldsymbol{x}(i)\equiv[x_{1,1}(i)\ x_{1,2}(i)\ \ldots\ x_{K,L}(i)]^T\in\mathbb{C}^{KL\times 1}$ becomes

$$\begin{aligned}\boldsymbol{x}(i) &= \mathbf{D}_W\cdot\mathbf{r}_W(i) \\ &= \mathbf{S}_W\cdot\mathbf{b}_W(i)+\mathbf{D}_W\cdot\mathbf{n}_W(i) \\ &= \boldsymbol{b}(i)+\boldsymbol{z}_W(i), \end{aligned} \tag{13}$$

where $\boldsymbol{z}_W(i)$ is a decorrelator noise vector, which is Gaussian since it is a linear transformation of Gaussian noise $\mathbf{n}_W(i)$. Its covariance matrix is

$$E[\boldsymbol{z}_W(i)\cdot\boldsymbol{z}_W^H(i)]=\sigma^2\mathbf{S}_W\cdot\mathbf{R}_W^{-1}\cdot\mathbf{S}_W^T. \tag{14}$$

As shown in (13), the decorrelator output vector $\boldsymbol{x}(i)$ consists of the desired signal vector $\boldsymbol{b}(i)$ and Gaussian noise vector $\boldsymbol{z}_W(i)$. In the FIR-DD, on the other hand, MAI components still remain on decorrelator outputs [8].

The decorrelator output vector in (13) has KL elements for K users. There are L elements for each user which are associated with L resolvable independently faded paths. These L elements are coherently combined to form a decision statistic $\Lambda_k(i)$ for user k, as follows:

$$\Lambda_k(i)=\sum_{l=1}^{L}a_{k,l}x_{k,l}(i)h_{k,l}^*(i), \tag{15}$$

where $a_{k,l}$ is a combining coefficient and the asterisk denotes a complex conjugate.

3.3 Complexity Issue

In this subsection, we present and compare the complexities of EOS-DD, OS-DD, and FIR-DD. EOS-DD or FIR-DD requires only one decorrelator for the i-th symbols of all users, whereas OS-DD requires one decorrelator for i-th symbols of each user's each path, as mentioned previously. In decorrelating detectors, the matrix inversion for the decorrelating matrix $\mathbf{R}_W^{-1}$ is computationally more demanding than other operations in the receiver, and determines the computational complexity order. For this reason, we present computational complexity of matrix inversion as a measure of the total complexity. In the case of an $A\times A$ square matrix, the complexity of matrix inversion is $\mathcal{O}(A^3)$, which indicates that the complexity is proportional to A^3. Since the number of MF outputs used

in decorrelating process is equal to the number of rows or columns in decorrelating matrix, the complexities for one decorrelator of OS-DD, EOS-DD with window size $2W$ and FIR-DD with window size $2W+1$ are, respectively, $\mathcal{O}((2KL-1)^3)$, $\mathcal{O}(((2W+1)KL)^3)$, and $\mathcal{O}(((2W+1)KL)^3)$. Since OS-DD needs KL decorrelators for i-th symbols, total complexity for matrix inversion in OS-DD is $\mathcal{O}(KL(2KL-1)^3)$. It can be easily observed that the complexity of OS-DD increases more rapidly with the number of users or that of paths than other detectors. If W in EOS-DD and FIR-DD are the same, the complexity orders of both detectors are the same. When W increases into $W+1$ in the EOS-DD, the complexity increases by a factor of $(2W+3)^3/(2W+1)^3$. For example, the complexity of EOS-DD with window size 4 is about 5 times greater than that of EOS-DD with window size 2.

4. Analysis

In this section, the BER of EOS-DD is analyzed, and the effects of window size on performance are investigated from the viewpoint of noise power.

4.1 BER Analysis

The decision statistic $\Lambda_k(i)$ in (15) may be rewritten in quadratic form, and then it is expressed as

$$\Lambda_k(i) = \zeta_k(i)^H \cdot \Psi \cdot \zeta_k(i), \tag{16}$$

where $\zeta_k(i)$ is $[\breve{x}_{k,1}(i)\ \breve{x}_{k,2}(i)\ \ldots\ \breve{x}_{k,L}(i)\ h_{k,1}(i)\ h_{k,2}(i)\ \ldots\ h_{k,L}(i)]^T$ and $\breve{x}_{k,l}(i)$ denotes $a_{k,l}x_{k,l}(i)$. Ψ is defined as

$$\Psi \equiv \frac{1}{2}\begin{bmatrix} \mathbf{O}_{L\times L} & \mathbf{I}_{L\times L} \\ \mathbf{I}_{L\times L} & \mathbf{O}_{L\times L} \end{bmatrix}. \tag{17}$$

If the data is BPSK-modulated, then the BER can be calculated as [11]

$$P_e = \sum_{\lambda_m<0} \prod_{\substack{n=1 \\ n\neq m}}^{2L} \frac{1}{1-\lambda_n/\lambda_m}, \tag{18}$$

where $\{\lambda_m, m=1,2,\ldots,2L\}$ are the eigenvalues of $\Gamma\cdot\Psi$ and Γ is the correlation matrix of $\zeta_k(i)$.

$$\Psi = E[\zeta_k(i)\cdot\zeta_k(i)^H] = \begin{bmatrix} \Gamma_{11} & \Gamma_{12} \\ \Gamma_{21} & \Gamma_{22} \end{bmatrix}, \tag{19}$$

where

$$\begin{aligned}
\Gamma_{11(u,v)} &= E[\breve{x}_{k,u}(i)\cdot\breve{x}^*_{k,v}(i)] \\
&= a_{k,u}a_{k,v}\frac{\delta_{uv}+\sigma^2(\mathbf{U}_W)_{(kL+u,kL+v)}}{(\mathbf{U}_W)_{(kL+u,kL+u)}\cdot(\mathbf{U}_W)_{(kL+v,kL+v)}}, \\
\Gamma_{12(u,v)} &= E[\breve{x}_{k,u}(i)\cdot h^*_{k,v}(i)] \\
&= \frac{a_{k,u}\delta_{uv}}{(\mathbf{U}_W)_{(kL+u,kL+u)}}, \\
\Gamma_{21} &= \Gamma_{12}^H, \\
\Gamma_{22(u,v)} &= E[h_{k,u}(i)\cdot h^*_{k,v}(i)] = \delta_{uv}, \\
\mathbf{U}_W &\equiv \mathbf{S}_W\cdot\mathbf{R}_W^{-1}\cdot\mathbf{S}_W^T,
\end{aligned} \tag{20}$$

δ_{uv} is the Kronecker delta function, and $A_{(a,b)}$ denotes the element of A at the a-th row and the b-th column.

4.2 Noise Power Analysis

In this subsection, the effects of window size on performance are investigated. Since EOS-DD eliminates MAI completely as indicated in (13), the performance of EOS-DD depends not on MAI but on noise components. Note that the decorrelator changes the noise power of a signal, and the noise power variation is related with window size. Since the received signal power does not change, the effects of window size on performance may be investigated in terms of the variation of noise power. To obtain insights, we define a normalized noise power as the ratio of the noise power of decorrelator output to that of the matched-filter output, and investigate the effects of window size on performance in terms of the normalized noise power.

From (5) and (14), the normalized noise power for the k-th user's l-th path is denoted as

$$\begin{aligned}
\frac{E[|z_{k,l}(i)|^2]}{E[|n_{k,l}(i)|^2]} &= \frac{(E[\boldsymbol{z}_W(i)\cdot\boldsymbol{z}_W(i)^H])_{(kL+l,kL+l)}}{(E[\boldsymbol{n}(i)\cdot\boldsymbol{n}(i)^H])_{(kL+l,kL+l)}} \\
&= \frac{\sigma^2\cdot(\mathbf{S}_W\cdot\mathbf{R}_W^{-1}\cdot\mathbf{S}_W^T)_{(kL+l,kL+l)}}{\sigma^2\cdot\mathbf{R}(0)_{(kL+l,kL+l)}} \\
&= (\mathbf{S}_W\cdot\mathbf{R}_W^{-1}\cdot\mathbf{S}_W^T)_{(kL+l,kL+l)}.
\end{aligned} \tag{21}$$

Hence, the properties of $\mathbf{S}_W\cdot\mathbf{R}_W^{-1}\cdot\mathbf{S}_W^T$ are investigated to examine the window size effect.

Firstly, we show that $(\mathbf{S}_W\cdot\mathbf{R}_W^{-1}\cdot\mathbf{S}_W^T)^{-1}$ is symmetric and positive semidefinite (S.P.S.) [12] for all $W\geq 1$. The properties of S.P.S. are summarized in Appendix A. The S.P.S. property of $(\mathbf{S}_W\cdot\mathbf{R}_W^{-1}\cdot\mathbf{S}_W^T)^{-1}$ is proven as follows. Since $\mathbf{R}_W$ is defined as $\int_{-\infty}^{\infty}\mathbf{s}_W(i,t)\cdot\mathbf{s}_W(i,t)^T dt$, $\mathbf{R}_W$ is S.P.S. by Property (1) in Appendix A. Its inverse matrix $\mathbf{R}_W^{-1}$ is also S.P.S. by Property (3), and its principal submatrix $\mathbf{S}_W\cdot\mathbf{R}_W^{-1}\cdot\mathbf{S}_W^T$ is also by Property (4). Therefore, its inverse matrix, $(\mathbf{S}_W\cdot\mathbf{R}_W^{-1}\cdot\mathbf{S}_W^T)^{-1}$ is S.P.S. by Property (3).

Secondly, we show that $(\mathbf{S}_{W+1}\cdot\mathbf{R}_{W+1}^{-1}\cdot\mathbf{S}_{W+1}^T)^{-1} - (\mathbf{S}_W\cdot\mathbf{R}_W^{-1}\cdot\mathbf{S}_W^T)^{-1}$ is also S.P.S. for all $W\geq 1$. By definition, $\mathbf{D}_W\equiv\mathbf{S}_W\cdot\mathbf{R}_W^{-1}$ should satisfy the following equation.

$$\begin{aligned}
\mathbf{D}_W\cdot\mathbf{R}_W &= \mathbf{S}_W \\
&= [\mathbf{0}_{KL\times WKL}\ \mathbf{I}_{KL\times KL}\ \mathbf{0}_{KL\times WKL}]
\end{aligned} \tag{22}$$

From this equation, $\mathbf{S}_W\cdot\mathbf{R}_W^{-1}\cdot\mathbf{S}_W^T$, may be expressed as

$$\mathbf{S}_W\cdot\mathbf{R}_W^{-1}\cdot\mathbf{S}_W^T = (\mathbf{A}_W+\mathbf{B}_W-\mathbf{R}(0))^{-1}, \tag{23}$$

where

$$\mathbf{A}_{W+1} = \mathbf{R}(0) - \mathbf{R}(1) \cdot \mathbf{A}_W^{-1} \cdot \mathbf{R}(-1),$$
$$\mathbf{B}_{W+1} = \mathbf{R}(0) - \mathbf{R}(-1) \cdot \mathbf{B}_W^{-1} \cdot \mathbf{R}(1),$$
$$\mathbf{A}_0 = \tilde{\mathbf{R}}(0), \qquad \mathbf{B}_0 = \hat{\mathbf{R}}(0). \tag{24}$$

Then,

$$(\mathbf{S}_{W+1} \cdot \mathbf{R}_{W+1}^{-1} \cdot \mathbf{S}_{W+1}^T)^{-1} - (\mathbf{S}_W \cdot \mathbf{R}_W^{-1} \cdot \mathbf{S}_W^T)^{-1} = (\mathbf{A}_{W+1} - \mathbf{A}_W) + (\mathbf{B}_{W+1} - \mathbf{B}_W). \tag{25}$$

According to Appendix B, $\mathbf{A}_{W+1} - \mathbf{A}_W$ and $\mathbf{B}_{W+1} - \mathbf{B}_W$ are S.P.S. Hence, their sum $(\mathbf{A}_{W+1} - \mathbf{A}_W) + (\mathbf{B}_{W+1} - \mathbf{B}_W)$ is also S.P.S. by Property (2). As a result, $(\mathbf{S}_{W+1} \cdot \mathbf{R}_{W+1}^{-1} \cdot \mathbf{S}_{W+1}^T)^{-1} - (\mathbf{S}_W \cdot \mathbf{R}_W^{-1} \cdot \mathbf{S}_W^T)^{-1}$ is S.P.S. for all $W \geq 1$.

Finally, using the above results and Property (5), the following statement is obtained.

$$(\mathbf{S}_W \cdot \mathbf{R}_W^{-1} \cdot \mathbf{S}_W^T - \mathbf{S}_{W+1} \cdot \mathbf{R}_{W+1}^{-1} \cdot \mathbf{S}_{W+1}^T) \text{ is S.P.S. for all } W \geq 1 \tag{26}$$

If the matrix is S.P.S., then the diagonal elements of the matrix are nonnegative:

$$(\mathbf{S}_W \cdot \mathbf{R}_W^{-1} \cdot \mathbf{S}_W^T)_{(kL+l,kL+l)} \geq (\mathbf{S}_{W+1} \cdot \mathbf{R}_{W+1}^{-1} \cdot \mathbf{S}_{W+1}^T)_{(kL+l,kL+l)} \tag{27}$$

for any k, l, and $W \geq 1$. Since $(\mathbf{S}_W \cdot \mathbf{R}_W^{-1} \cdot \mathbf{S}_W^T)_{(kL+l,kL+l)}$ is the normalized noise power of the EOS-DD with window size $2W$, (27) indicates that the noise power for any user and path decreases as the window size of the decorrelator increases.

5. Numerical Results

In this section, the performance of EOS-DD is analyzed and verified by computer simulation, and compared with the performance of the conventional MF detector (MFD), FIR-DD, and OS-DD. The channel characteristics are assumed to be known. Data symbols are BPSK-modulated and BPSK-spread using the Gold code with period 31. Carrier frequency, vehicular speed and data rate are respectively 900 MHz, 60 mph, and 9600 bps and thus the normalized maximum Doppler frequency is 0.0083. The maximal ratio combining is used for diversity combining.

The BER of each detector as a function of SNR is plotted in Fig. 3. In this figure, K and L are respectively 20 and 2 and all of the user's signals are assumed to have the same average signal power. As shown in Fig. 3, EOS-DD is shown to outperform MFD and OS-DD, and BER performance of EOS-DD improves according to increment of W. The required SNRs for BER of 0.01 are 18.3, 15.0, 13.5 and 13.5 dB respectively for OS-DD and EOS-DD with W =1, 2 and 3. The reason for this is that EOS-DD does not enhance noise components as much as OS-DD does and that as W increases, noise enhancement of EOS-DD becomes small.

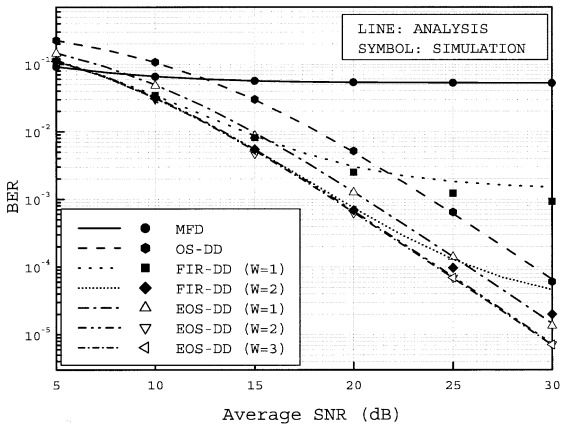

Fig. 3 BER versus average SNR (K=20 and L=2).

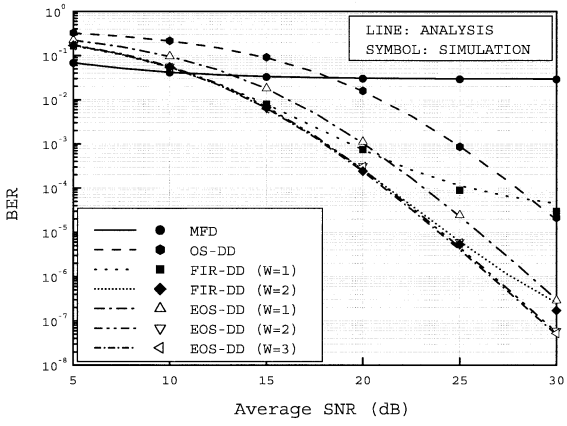

Fig. 4 BER versus average SNR (K=20 and L=4).

The difference in BER performance between EOS-DD and FIR-DD depends on SNR and W. When W in each detector is 1, EOS-DD outperforms FIR-DD at high SNR. The reason is that at high SNR, the complete elimination of interfering signal by EOS-DD with relatively large noise enhancement is more effective in BER performance than the partial elimination of interfering signal by FIR-DD with small noise enhancement. At low SNR, since noise has dominant effect on the BER performance, the BER of EOS-DD is slightly higher than that of FIR-DD. When W changes into 2, the performance difference becomes small compared to the case of $W = 1$. The reason is that BER of EOS-DD as well as FIR-DD approaches BER of IIR-DD, as W increases. At high SNR, however, the performance difference is considerable due to residual MAI, even if W is 2.

Figure 4 shows the performance of EOS-DD and those of other schemes when the number of resolvable paths is 4. The SNR gain of EOS-DD with $W = 2$ over EOS-DD with $W = 1$ is about 2.0 dB when BER is 0.01. Comparing Figs. 3 and 4, it is observed that the performance improvement of EOS-DD due to window size extension becomes large as the number of resolvable

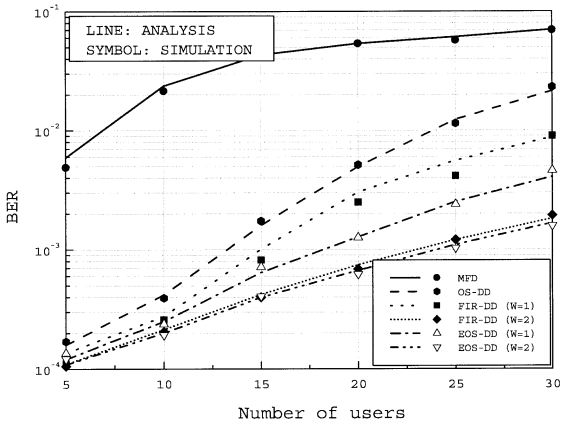

Fig. 5 BER versus number of users (L=2 and average SNR=20 dB).

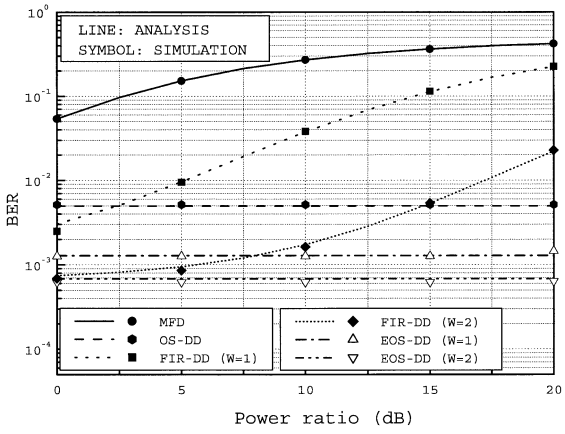

Fig. 6 BER versus power ratio (K=20, L=2, and average SNR=20 dB).

paths increases.

The effects of the number of users on BER performance is shown in Fig. 5. The number of resolvable paths is assumed to be 2 and the average SNR of each user is fixed at 20 dB. As shown in this figure, EOS-DD and FIR-DD outperforms OS-DD, and the BER performance of EOS-DD is better than that of FIR-DD if W is the same. As the number of users increases, the effects of noise enhancement and residual MAI also increase, and thus the performance difference between detectors becomes large, and the benefits of EOS-DD becomes noticeable.

Figure 6 shows how the performance varies with the ratio of an average interfering signal power P_{int} to an average desired signal power P_{des}. In this figure, the average powers of all interfering signals are assumed to be equal and the SNR for a desired signal is set to 20 dB. As expected, the BER performance of EOS-DD and OS-DD is robust to the variation of the interfering signal power, whereas that of MFD and FIR-DD is severely degraded as the power of interfering signal increases.

As investigated in Sect. 4, the performance of EOS-DD depends on the noise power variation through the decorrelator, and the noise power decreases as the window size increases. According to simulation results, when K and L are respectively 20 and 2, the average normalized noise power ratios $(\mathbf{S}_1 \cdot \mathbf{R}_1^{-1} \cdot \mathbf{S}_1^T)_{(kL+l,kL+l)}/(\mathbf{S}_2 \cdot \mathbf{R}_2^{-1} \cdot \mathbf{S}_2^T)_{(kL+l,kL+l)}$ and $(\mathbf{S}_2 \cdot \mathbf{R}_2^{-1} \cdot \mathbf{S}_2^T)_{(kL+l,kL+l)}/(\mathbf{S}_3 \cdot \mathbf{R}_3^{-1} \cdot \mathbf{S}_3^T)_{(kL+l,kL+l)}$ are 1.154 dB and 0.069 dB respectively. This means that the performance improvements by expanding the window size from 2 to 4 are significant, while on the other hand, the performance improvements are negligibly small even if the window size increases from 4 and 6. Other simulation results show similar trends even when the number of users and the number of resolvable paths change.

6. Conclusions

In this paper, the extended one-shot decorrelating detector (EOS-DD) is proposed. The EOS-DD can eliminate MAI completely while keeping noise power low with reasonably small window size. EOS-DD has near-far resistance and outperforms OS-DD and FIR-DD, and considerable performance improvement is achieved by extending the window size, with a small increase in complexity.

References

[1] S. Verdú, "Minimum probability of error for asynchronous Gaussian multiple-access channels," IEEE Trans. Inf. Theory, vol.IT-32, no.1, pp.85–96, Jan. 1986.
[2] S. Verdú, Recent Progress in Multiuser Detection: Advance in Communication and System, Springer Verlag, 1988.
[3] R. Lupas and S. Verdú, "Linear multiuser detectors for synchronous code-division multiple-access channels," IEEE Trans. Inf. Theory, vol.35, no.1, pp.123–136, Jan. 1989.
[4] R. Lupas and S. Verdú, "Near-far resistance of multiuser detectors in asynchronous channels," IEEE Trans. Commun., vol.38, no.4, pp.496–508, April 1990.
[5] Z. Xie, R.T. Short, and C.K. Rushforth, "A family of suboptimum detectors for coherent multi-user communications," IEEE J. Sel. Areas Commun., vol.8, no.4, pp.683–690, May 1990.
[6] P. Patel and J. Holtzman, "Analysis of a simple successive interference cancellation scheme in a DS/CDMA system," IEEE J. Sel. Areas Commun., vol.12. no.5, pp.796–807, June 1994.
[7] M.K. Varanasi and B. Aazhang, "Multistage detection in asynchronous code-division multiple-access communications," IEEE Trans. Commun., vol.38, no.4, pp.509–519, April 1990.
[8] M.J. Juntti and B. Aazhang, "Finite memory-length linear multiuser detection for asynchronous CDMA communications," IEEE Trans. Commun., vol.45, no.5, pp.611–622, May 1997.
[9] S. Verdú, Multiuser Detection, Cambridge Univ. Press, Cambridge, U.K., 1998.
[10] S.J. Baines, A.G. Burr, and T.C. Tozer, "Double window multi-user detection for asynchronous DS-CDMA," IEE Electronics Letters, vol.32, no.24, pp.2199–2201, Nov. 1996.

[11] M.J. Barrett, "Error probability for optimal and suboptimal quadratic receivers in rapid Rayleigh fading channels," IEEE J. Sel. Areas Commun., vol.SAC-5, no.2, pp.302–304, Feb. 1987.
[12] S.H. Friedberg, A.J. Insel, and L.E. Spence, Linear Algebra, 3rd ed., Prentice-Hall, Upper Saddle River, NJ, 1997.
[13] S.J. Meang, Extended window decorelating detection methods for DS/CDMA channels, Ph.D. Dissertation, Seoul National University, Seoul, Korea, 1998.

Appendix A

The S.P.S. matrix has the following properties [12], [13].

(1) $\mathbf{A}$ is S.P.S., if $\mathbf{A} = \int \mathbf{B}(y) \cdot \mathbf{B}(y)^T dy$ for any matrix $\mathbf{B}(y)$. (A·1)

(2) If $\mathbf{A}$ and $\mathbf{B}$ are S.P.S., $\mathbf{A}+\mathbf{B}$ is S.P.S. (A·2)

(3) If $\mathbf{A}$ is S.P.S., $\mathbf{A}^{-1}$ is S.P.S. (A·3)

(4) If $\mathbf{A}$ is S.P.S., any principal submatrix of $\mathbf{A}$ is S.P.S. (A·4)

(5) If $\mathbf{A}$, $\mathbf{B}$, and $\mathbf{A}-\mathbf{B}$ are S.P.S., $\mathbf{B}^{-1}-\mathbf{A}^{-1}$ is S.P.S. (A·5)

Appendix B

In this appendix, it will be proven that $\mathbf{A}_{W+1}-\mathbf{A}_W$ and $\mathbf{B}_{W+1}-\mathbf{B}_W$ are S.P.S. for $W \geq 1$. First, the symmetry and positive semidefiniteness of $\mathbf{A}_{W+1}-\mathbf{A}_W$ are induced by the following lemma.

Lemma.
a) $\mathbf{A}_1-\mathbf{A}_0$ is S.P.S.
b) If $\mathbf{A}_W-\mathbf{A}_{W-1}$ is S.P.S., then $\mathbf{A}_{W+1}-\mathbf{A}_W$ is S.P.S. for $W \geq 1$.

Proof of Lemma a)

By the definition of $\mathbf{A}_W$,

$$\begin{aligned}\mathbf{A}_1-\mathbf{A}_0 &= \mathbf{R}(0)-\mathbf{R}(1)\cdot\tilde{\mathbf{R}}(0)^{-1}\cdot\mathbf{R}(-1)-\tilde{\mathbf{R}}(0)\\ &= \hat{\mathbf{R}}(0)-\mathbf{R}(1)\cdot\tilde{\mathbf{R}}(0)^{-1}\cdot\mathbf{R}(-1). \quad (\text{A}\cdot 6)\end{aligned}$$

To prove that $\hat{\mathbf{R}}(0)-\mathbf{R}(1)\cdot\tilde{\mathbf{R}}(0)^{-1}\cdot\mathbf{R}(-1)$ is S.P.S, the new matrix $\mathcal{R}$ is introduced.

$$\mathcal{R} \equiv \begin{bmatrix} \tilde{\mathbf{R}}(0) & \mathbf{R}(-1) \\ \mathbf{R}(1) & \hat{\mathbf{R}}(0) \end{bmatrix} \quad (\text{A}\cdot 7)$$

Since $\mathcal{R}$ can be represented as

$$\mathcal{R} = \int_{-\infty}^{\infty} \begin{bmatrix} \tilde{\boldsymbol{s}}(i-1,t) \\ \hat{\boldsymbol{s}}(i,t) \end{bmatrix} \cdot [\tilde{\boldsymbol{s}}(i-1,t)^T \ \hat{\boldsymbol{s}}(i,t)^T] dt, \quad (\text{A}\cdot 8)$$

$\mathcal{R}$ is S.P.S. by Property (1). Hence, $(\hat{\mathbf{R}}(0)-\mathbf{R}(1)\cdot\tilde{\mathbf{R}}(0)^{-1}\cdot\mathbf{R}(-1))^{-1}$, the principal submatrix of $\mathcal{R}^{-1}$ is also S.P.S., which means that its inverse matrix, $\hat{\mathbf{R}}(0)-\mathbf{R}(1)\cdot\tilde{\mathbf{R}}(0)^{-1}\cdot\mathbf{R}(-1)$ is S.P.S.

Proof of Lemma b)

By the definition of $\mathbf{A}_W$,

$$\mathbf{A}_{W+1}-\mathbf{A}_W = \mathbf{R}(1)\cdot(\mathbf{A}_{W-1}^{-1}-\mathbf{A}_W^{-1})\cdot\mathbf{R}(-1) \quad (\text{A}\cdot 9)$$

for $W \geq 1$. In (A·9), since $\mathbf{R}(-1)=\mathbf{R}(1)^T$,

$$\mathbf{A}_{W-1}^{-1}-\mathbf{A}_W^{-1} \text{ is S.P.S.} \Rightarrow \mathbf{A}_{W+1}-\mathbf{A}_W \text{ is S.P.S.} \quad (\text{A}\cdot 10)$$

Since $\mathbf{A}_0=\tilde{\mathbf{R}}(0)$ is S.P.S. by Property (1) in Appendix A and $\mathbf{A}_{W+1}$ is $\mathbf{R}(0)-\mathbf{R}(1)\cdot\mathbf{A}_W^{-1}\cdot\mathbf{R}(-1)$, $\mathbf{A}_W$ is S.P.S. for all $W \geq 1$ by Properties (2), (3), and (4). Hence, the S.P.S. of $\mathbf{A}_{W-1}^{-1}-\mathbf{A}_W^{-1}$ is equivalent to the S.P.S. of $\mathbf{A}_W-\mathbf{A}_{W-1}$ by Property (5). As a result,

$$\mathbf{A}_W-\mathbf{A}_{W-1} \text{ is S.P.S.} \Rightarrow \mathbf{A}_{W+1}-\mathbf{A}_W \text{ is S.P.S.} \quad (\text{A}\cdot 11)$$

for $W \geq 1$.

By lemmas a) and b), $\mathbf{A}_{W+1}-\mathbf{A}_W$ is S.P.S. for $W \geq 0$ and, of course, for $W \geq 1$. The symmetry and positive semidefiniteness of $\mathbf{B}_{W+1}-\mathbf{B}_W$ can be proven in the same manner.

Jee Woong Kang was born in Seoul, Korea, in 1975. He received the B.S. and M.S. degrees in electrical engineering from Seoul National University, Seoul, Korea, in 1998 and 2000, respectively. He is currently working towards the Ph.D. degree in electrical engineering at Seoul National University. His current research interests include mobile communications, spread spectrum, multiuser detector, and multi-input multi-output systems.

Kwang Bok (Ed) Lee received the B.A.Sc. and M.Eng. degrees from the University of Toronto, Toronto, Ont., Canada, in 1982 and 1986, respectively, and the Ph.D. degree from McMaster University, Canada in 1990. He was with Motorola Canada from 1982 to 1985, and Motorola USA from 1990 to 1996 as a Senior Staff Engineer. At Motorola, he was involved in the research and development of wireless communication systems. He was with Bell-Northern Research, Canada, from 1989 to 1990. In March 1996, he joined the School of Electrical Engineering, Seoul National University, Seoul, Korea. Currently he is an Associate Professor and Vice Chair in the School of Electrical Engineering. He has been serving as a Consultant to a number of wireless industries. His research interests include mobile communications, communication theories, spread spectrum, and signal processing. He holds twelve U.S. patents, three European patents, three Chinese patents, two Korean patents, and two Japanese patents, and has a number of patents pending. Dr. Lee is serving as an Associate Editor of the IEEE TRANSACTIONS ON WIRELESS COMMUNICATIONS. He received the Best Paper Award from CDMA International Conference 2000 (CIC 2000).